COMPUTATIONAL METHODS IN ENGINEERING
3rd Asia-Pacific Int. Conf. on Comp. Meth. in Engrg (ICOME 2009)
Oct. 18-20, 2009, Nanjing, China

Fast Multipole Boundary Element Method in Rolling Engineering and its Research Progress

G. X. Shen [1]*, C. X. Yu [2], D. Y. Liu [3]

[1] *College of Mechanical Engineering, Yanshan University, Qinhuangdao, 066004 China*
[2] *College o f Science, Yanshan University, Qinhuangdao, 066004 China*
[3] *Beijing JieRuiTe Company, Beijing, 100088 China*

Email: sgx35@ysu.edu.cn

Abstract The FM-BEM and its research progress in rolling engineering are systematically introduced. At first, the principle and mathematical theory of the FM-BEM is demonstrated. Secondly, numerical computations for the FM-BEM are analyzed. Some fundamental functions and formulae are constructed for the boundary surface. An optimization mathematical model is established for the elastic and elasto-plastic frictional contact system. Practical and efficient solution strategies and algorithm are presented. Thirdly, some applications of FM-BEM in large-scale rolling engineering are presented, which includes the simulations of roll shape, stand stress, assembly process of the oil film bearing tapered sleeve and roll neck, reliability of the 3500mm mill pressure screw-pairs, and cold-rolling process of 2030mm four-high mill. Finally, the development trend and some problems to solve are discussed.

Key words: FM-BEM, rolling engineering, optimization model, IGMRES(m), elastic and elasto-plastic

1 INTRODUCTION

In the fields of aeronautics and astronautics, mechanics and civil engineering, many frictional contact problems involve multiple bodies and nonlinear factors, for which the numerical solution is very difficult[1-2]. For example, the four-high mill strip rolling process, the numerical analysis and simulations are almost impossible without new efficient theories and methods. So, it has become an urgent subject and task to find suitable numerical methods and techniques for the large-scale frictional contact problems with complicated calculations.

However, The Fast Multipole Method (FMM) was considered as one of the ten distinguished scientific calculation algorithms in 20 century[3]. Combined with the FMM, the conventional Boundary Element Method (BEM) could be used to efficiently solve large-scale frictional contact problems and it had obtained a great progress in theory and application, which directly resulted in the formation and development of a new Fast Multipole Boundary Element Method (FM-BEM)[4-10]. Based on the Generalized Minimal Residual (GMRES) algorithm [6], the FM-BEM aims at the solution of large scale problems and the improvement of computational efficiency. Now it has become one of the most popular numerical methods and has been extensively applied in computational mathematics and mechanics, mechanical engineering, acoustics, and numerical simulations of composite materials and complicated engineering problems with highly nonlinear factors.

In authors' group, the investigations on the FM-BEM started in 2001. Some exploratory and productive works in theory, in numerical methods and in applications have been made in recent years [5-7, 11-18]. The purpose of this paper is to systematically introduce some of our results about the FM-BEM and its research

progress in rolling engineering field, including the principle, mathematical theory, optimization model, numerical formulae and algorithms, and some large-scale numerical simulations of complicated frictional contact systems.

2 FUNDAMENTAL PRINCIPLES FOR THE FM-BEM

2.1 Combination point for the FMM and BEM

FMM originates in the computation of electrostatic field. It can be used to compute the interaction of quantity particles. These particles are divided into different sets according to their spatial locations. When a set is far away from another set, the interaction of their particles is computed by using the FMM. Otherwise, it is directly computed. In addition, direct computation is also used to compute the interaction of two particles that are in the same set. The FMM expression is as follows:

$$\Phi(X_j)=\sum_{\substack{i=1\\ i\neq j}}^{n}\frac{q_i}{\left\|X_j-X_i\right\|} \tag{1}$$

where $X_1, X_2, \ldots, X_n$ indicate the points in R^3, and $q_1, q_2, \ldots, q_n$ are a group of constants related with $X_1, X_2, \ldots, X_n$.

Combined with the FMM, the BEM has been developed into the FM-BEM. The root reason is the FMM can be used to fast compute the far influence coefficients in the BEM. The key to establish the FM-BEM is the BEM fundamental solutions can be decomposed into the FMM expressions. In the FMM, we find that Eq.(1) can be reduced to a general mathematical formula $\sum_{i\neq j}\frac{c_i}{R_{ij}}$ (R_{ij} indicates the distance between two arbitrary particles, and c_i is a constant that indicates the quantity of electricity for a particle). While in the BEM, the discrete expressions for the boundary integral equations can also be reduced to the general formula $\sum_{i\neq j}\frac{c_i}{R_{ij}}$ (R_{ij} indicates the distance between a source point and an integral point, and c_i is an influence coefficient that indicates the interaction between the source point and the integral point) or its partial derivatives. For example, the final discrete expression for the boundary integral equation of the elastic problems is as follows:

$$\begin{aligned}
&c_{ij}\,u_j(x^q)+R_{ijm}(x^q)\sum_{k,l,s}\frac{1}{\left|x^q-y_c\right|}\left\{u_j^{kl}\phi^l(\xi^s)n_m[y(\xi^s)]J[y(\xi^s)]\omega^s\right\}+\\
&S_{im}(x^q)\sum_{k,l,s}\frac{1}{\left|x^q-y_c\right|}\left\{u_j^{kl}\phi^l(\xi^s)\,n_m[y(\xi^s)]\,y_j(\xi^s)\,J[y(\xi^s)]\,\omega^s\right\}-\\
&P_{ij}(x^q)\sum_{k,l,s}\frac{1}{\left|x^q-y_c\right|}\left\{t_j^{kl}\,\phi^l(\xi^s)\,J[y(\xi^s)]\,\omega^s\right\}-\\
&Q_i(x^q)\sum_{k,l,s}\frac{1}{\left|x^q-y_c\right|}\left\{t_j^{kl}\,\phi^l(\xi^s)\,y_j(\xi^s)\,J[y(\xi^s)]\,\omega^s\right\}=0
\end{aligned} \tag{2}$$

where x^q indicates the source point, $R=\left|x^q-y_c\right|$ the distance between the source point and a multipole center, $R_{ijm}(x^q)$, $S_{im}(x^q)$, $P_{ij}(x^q)$ and $Q_i(x^q)$ the operators of partial derivative, and $\left\{u_j^{kl}\phi^l(\xi^s)n_m[y(\xi^s)]J[y(\xi^s)]\omega^s\right\}$, $\left\{u_j^{kl}\phi^l(\xi^s)\,n_m[y(\xi^s)]\,y_j(\xi^s)\,J[y(\xi^s)]\omega^s\right\}$, $\left\{t_j^{kl}\,\phi^l(\xi^s)\,J[y(\xi^s)]\omega^s\right\}$ and $\left\{t_j^{kl}\,\phi^l(\xi^s)\,y_j(\xi^s)\,J[y(\xi^s)]\omega^s\right\}$ the influence coefficients for the interactions of the source point and the multipole centers.

2.2 Equivalence of the fundamental solutions for the BEM and FM-BEM

To introduce the FMM into the BEM, fundamental solutions and kernel functions are appropriately decomposed [11]. The two kinds of solution are proved to be equivalent. To further demonstrate this equivalent relationship, some numerical examples are made for elastic problems.

For the fundamental solutions of displacements $U_{ij}(x,y)$ and tractions $T_{ij}(x,y)$, the conventional BEM solutions can be decomposed into FM-BEM format ones with two terms. If $i=j=1$, then $U_{11}(x,y)$ is shown in Fig.1. If $i=j=1$, $p=1,2,3$, then $T_{11}(x,y)$ is shown in Fig.2.

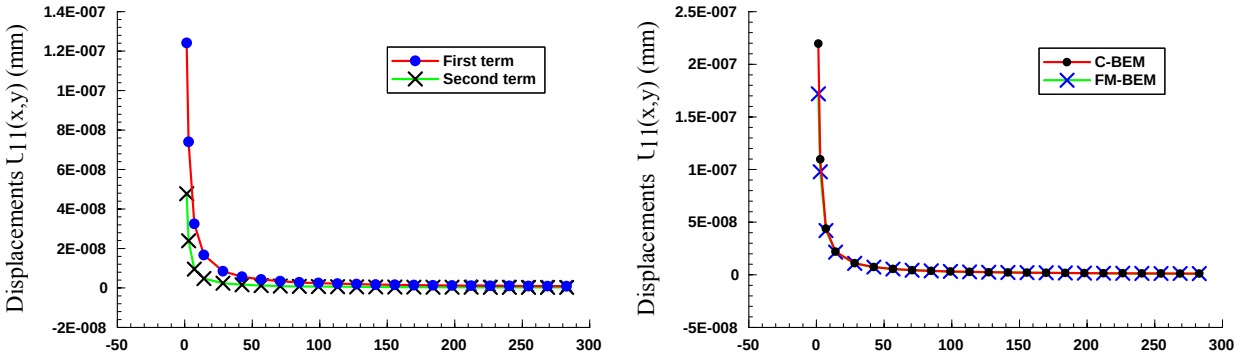

(a)FM-BEM format with two terms (b)Comparison of two kinds of format

Fig.1 Equivalence of solutions for $U_{11}(x,y)$

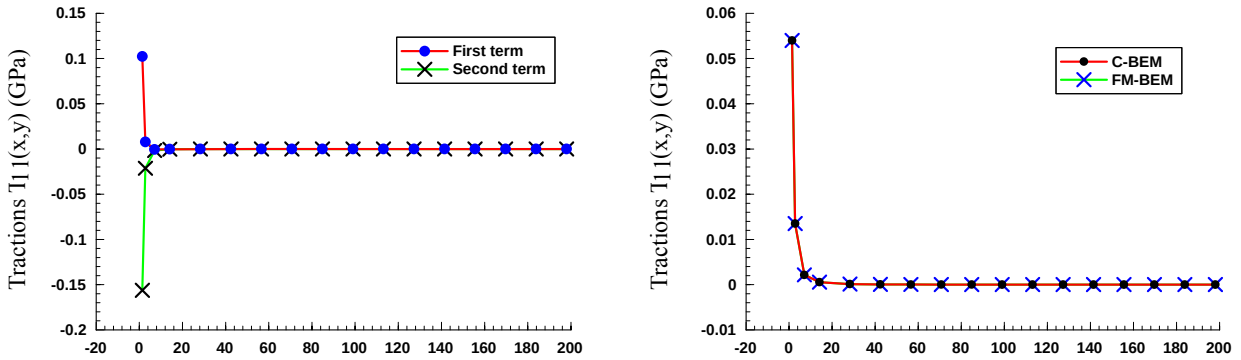

(a)FM-BEM format with two terms (b)Comparison of two kinds of format

Fig.2 Equivalence of solutions for $T_{11}(x,y)$

From Figs.1-2, we can see that the conventional BEM solutions and the FM-BEM ones are coherent in the numerical analysis. If r indicates the radius of the minimal set of integral points, and R the distance between the source point and the center of the object points set, then the two kinds of solutions are almost coincident when $R>3r$. It verifies that the introduction of FMM is very significant under the condition $R>3r$.

2.3 Existence and uniqueness of the solution for GMRES(m) based FM-BEM

GMRES(m) algorithm is usually used to well solve the frictional contact FM-BEM problems. In the solution process, the most important of all is the solution of the least squares problems, which can be expressed as[16]:

$$\min\left\|r^{(m)}\right\| = \min_{V_m y_m \in K_m} \left\|\beta v_1 - AV_m y_m\right\| \tag{3}$$

Let $AV_m = B, y_m = X = (x_1, x_2, \cdots x_m)^T, \beta v_1 = C,\ r_m = D$. From reference [16], $D = C - BX$ and Eq.(3) satisfies the following algebraic conditions:

$$B^T BX = B^T C \tag{4}$$

The linear equations Eq.(4) is the algebraic equation for the least squares solution, in which $B^T B$ and $B^T C$ are the coefficient matrix and the constant term, respectively.

Theorem 1[16]**.** Suppose that $B \in R^{n\times m}$, $n > m$, then $B^T B$ is a symmetric matrix.

Theorem 2[16]**.** For the matrix $B^T B$, there exists an orthogonal matrix $T \in R^{n\times n}$, which results in $T^T(B^T B)T = T^{-1}(B^T B)T = diag(\lambda_1, \lambda_2, \cdots, \lambda_n)$, where $\lambda_1, \lambda_2, \cdots, \lambda_n$ are the eigenvalues of $B^T B$.

Theorem 3[16]**.** Suppose that $B \in R^{n\times m}$, $n > m$, then $B^T B$ is positive definite.

From the above analysis, the equations of frictional contact system can be reduced to a simple system of equations

$$Ax = b \tag{5}$$

where $A = B^T B, b = B^T c, x = X$.

Theorem 4[16]. From Theorem 1-3, the FM-BEM solution of Eq.(5) is existent and unique.

3 OPTIMIZATION FM-BEM AND ITS NUMERICAL ALGORITHMS FOR THE ELASTIC AND ELASTO-PLASTIC FRICTIONAL CONTACT SYSTEM

3.1 Spherical harmonics and numerical formulae

In the FM-BEM, it is very important for the simulation to select a suitable spherical harmonic function. Some numerical formulae must be derived for the spherical harmonics.

From the Addition Formula **[13]**, we have

$$\frac{1}{\sin\theta}\frac{\partial}{\partial\theta}(\sin\theta\frac{\partial S}{\partial\theta}) + \frac{1}{\sin^2\theta}\frac{\partial^2 S}{\partial\varphi^2} + n(n+1)S = 0 \tag{6}$$

Or

$$\frac{\partial^2 S}{\partial\theta^2} + \cot\theta\frac{\partial S}{\partial\theta} + \frac{1}{\sin^2\theta}\frac{\partial^2 S}{\partial\varphi^2} + n(n+1)S = 0 \tag{6}*$$

The bounded (for θ) periodic (for φ) solutions totals $2n+1$ with $0 \le \varphi \le 2\pi$ and $0 \le \theta \le \pi$.

$$P_n^m(\cos\theta)e^{im\varphi}, \quad m = 0, \pm 1, \cdots, \pm n$$

Using Rodrigues formula[13], the associated Legendre function $P_n^m(x)$ can be proved to satisfy the relationship

$$P_n^{-m}(x) = (-1)^m \frac{(n-m)!}{(n+m)!} P_n^m(x) \tag{7}$$

and the orthogonal relation $(m, m' \ge 0)$.

$$\int_{-1}^{1} P_n^m(x) P_{n'}^m(x)\,dx = \frac{2}{2n+1}\frac{(n+m)!}{(n-m)!}\delta_{nn'} \tag{8}$$

In the FM-BEM, the spherical harmonic function

$$Y_{nm}(\theta,\varphi) = \sqrt{\frac{2n+1}{4\pi}\frac{(n-m)!}{(n+m)!}}\, P_n^m(\cos\theta)e^{im\varphi} \quad (m = 0, \pm 1, \cdots, \pm n) \tag{9}$$

is taken as the bounded periodic solution of Eq. (6), which satisfies the relationship

$$\int_0^{\pi}\int_0^{2\pi} Y_{nm}^{*} Y_{n'm'} \sin\theta \, d\varphi \, d\theta = \delta_{mm'}\delta_{nn'} \tag{10}$$

where Y_{nm}^{*} is the conjugate complex of Y_{nm}, and

$$Y_{nm}^{*} = (-1)^m Y_{n,-m} \tag{11}$$

Eq. (11) can be proved by Eq. (7). Eq. (10) can be proved by Eq. (8) and the following relationship:

$$\frac{1}{2\pi}\int_0^{2\pi} e^{-imx} e^{inx} dx = \delta_{mn} \quad (\rho(x) = 1) \tag{12}$$

However, Eq. (7) is required if $m < 0$ or $m' < 0$.

In the FM-BEM, Eq. (9) is the bond of spherical harmonic function and associated Legendre function. For the numerical computation of the spherical harmonic function $Y_{nm}(\theta, \varphi)$ in Eq. (9), the key point is the associated Legendre polynomial. There are many numerical methods to compute the associated Legendre polynomial. However, most of them are not too well. A more effective computational method is given as follows.

The associated Legendre polynomial satisfies many recurrence relationships, which can be with respect to n or m, or to both n and m. Most of them with respect to m are instable and not suitable for numerical computation. Using mathematical induction, $P_n^m(x)$ is proved to satisfy

$$(n-m) P_n^m(x) = (2n-1)\, x\, P_{n-1}^m(x) - (n+m-1)\, P_{n-2}^m(x) \tag{13}$$

which is stable with respect to n and also a practical numerical formula. It can be proved that $P_n^m(x)$ has closed expression

$$P_m^m(x) = (-1)^m (2m-1)!!(1-x^2)^{\frac{m}{2}} \tag{14}$$

with respect to initial values. For Eq. (13), let $n = m+1$, $P_{m-1}^m(x) = 0$, then

$$P_{m+1}^m(x) = (2m+1)\, x\, P_m^m(x) \tag{15}$$

In Eq. (13), the two initial values suitable for general n are given by Eqs. (14) and (15).

3.2 Practical strategies for the numerical integration

Compared with the conventional BEM, the FM-BEM shows obvious superiority in the computation of influence coefficients, as is shown in Fig. 3.

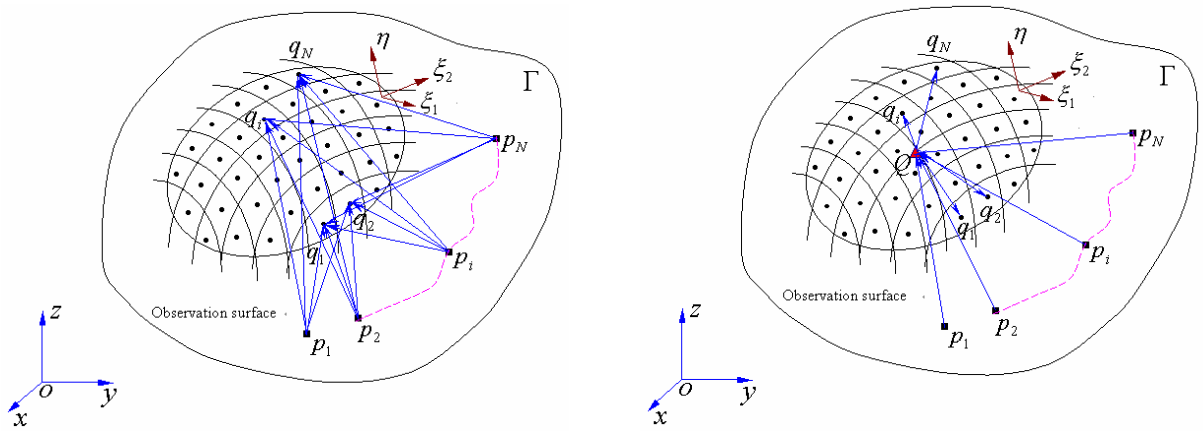

(a)Conventional BEM (b)FM-BEM

Fig. 3 Efficiency comparison for computing influence coefficients

In Fig. 3, q_i indicates the center of the i th element on the observation surface, p_i indicates the i th source node, and Q the multipole center. From Fig. 3, we can see that the operations can be approximately reduced from $O(N^2)$ to $O(N)$ if the FM-BEM is used in the computation of influence coefficients. The computational efficiency can be greatly improved.

3.3 Optimization mathematical model for the elastic and elasto-plastic frictional contact system

3.3.1 node-to-surface contact mode

To obtain the system of equations for the frictional contact system, it is necessary to discriminate the contact states from bodies A and B, for which the node-to-surface frictional contact model is used [5, 6].
The position of the elastic body is found during the solution process. Coordinates of the nodes will indicate when contact occurs. The two contact bodies should meet the constraint demands without penetration. P is an arbitrary point on object A, which is shown in Fig.4. (a) is the contact model and (b) is a partially enlarged detail. If P meets the conditions of Eq.(16), P is considered to be in contact with element S on object B. Element S is composed of four nodes (X_1, X_2, X_3, X_4).

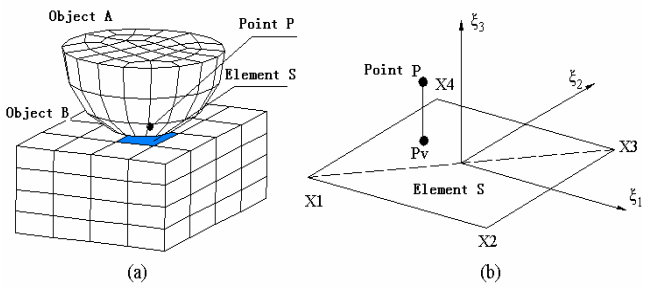

Fig.4 Node-to-surface contact model

$$\begin{cases} d \le \delta \\ \mathrm{P_V} \subset \Delta X_1 X_2 X_3 \ or\ \mathrm{P_V} \subset \Delta X_1 X_3 X_4 \end{cases} \tag{16}$$

where d indicates the distance between P and $\mathrm{P_V}$, $\mathrm{P_V}$ the pedal of P on element S, and δ the contact tolerance (defaulted as one hundredth of the length of the smallest element).

3.3.2 Establishment of the optimization mathematical model

For the contact bodies, when the boundaries are discretized, the total numbers of discrete nodes are N_A and N_B, respectively. The nodes on the contact surface are N_A^c and N_B^c, respectively. For each contact node of bodies A and B, three necessary equations are added through the linearization of the nonlinear contact constraints[6]. Then a node-to-surface optimization mathematical model can be established for the elastic frictional contact system, which is shown in Eq.(17)[14].

$$\begin{cases} \min \left\| F(x) \right\| \\ f_i^A(x) = 0 \quad (i = 1, 2, \cdots, 3N_A) \\ f_i^B(x) = 0 \quad (i = 1, 2, \cdots, 3N_B) \\ g_i^A(x) = 0 \quad (i = 1, 2, \cdots, 3N_A^c) \\ g_i^B(x) = 0 \quad (i = 1, 2, \cdots, 3N_B^c) \\ x = \{x_j\} \quad (j = 1, 2, \cdots, NF) \end{cases} \tag{17}$$

In Eq.(17), the objective function is a least squares residual modular function,

$$\| F(x) \| = \sqrt{\sum_{i=1}^{3N_B} [\, f_i^{\,B}(x)]^2 + \sum_{i=1}^{3N_B^c} \sum_{k=1}^{3} [\, g_{ik}^{B}(x)]^2 + \sum_{i=1}^{3N_A} [\, f_i^{\,A}(x)]^2 + \sum_{i=1}^{3N_A^c} \sum_{k=1}^{3} [\, g_{ik}^{A}(x)]^2}$$

$f_i^{\,A}(x)$ and $f_i^{\,B}(x)$ are two residual functions defined from the control equations for bodies A and B, respectively. $g_i^{\,A}(x)$ and $g_i^{\,B}(x)$ are two functions defined in the linearization of the nonlinear contact constraints for bodies A and B, respectively. Let $NF = 3(N_A + N_B + N_A^{\,c} + N_B^{\,c})$ be the total Degree Of Freedom(DOF). By using the GMRES(m) algorithm and least square method, the solution of the system equations reduces to $Ax = b$ [14].

3.4 Secondary optimization of the model

In the model expressed by Eq.(17), if the objective function $\| F(x) \|$ is replaced by the strictly convex quadratic function $\varphi(x) = \frac{1}{2}(Ax, x) - (b, x)$, then a new quadratic programming model for the frictional contact system can be established as follows:

$$\begin{cases} \min \varphi(x) \\ f_i^{\,A}(x) = 0 \quad (\, i = 1, 2, \cdots, 3N_A \,) \\ f_i^{\,B}(x) = 0 \quad (\, i = 1, 2, \cdots, 3N_B \,) \\ g_i^{\,A}(x) = 0 \quad (\, i = 1, 2, \cdots, 3N_A^{\,c} \,) \\ g_i^{\,B}(x) = 0 \quad (\, i = 1, 2, \cdots, 3N_B^{\,c} \,) \\ x = \{ x_j \} \quad (\, j = 1, 2, \cdots, NF) \end{cases} \tag{18}$$

It can be demonstrated that the optimum solution to the quadratic programming model expressed by Eq.(18) is existent and unique[16]. The optimality condition for the quadratic programming model is not only sufficient, but also necessary.

3.5 Fast solver: IGMRES(m) algorithm

By using the truncation technology, we proposed a fast Incomplete Generalized Minimal Residual (IGMRES(m)) algorithm based on the FM-BEM and established the convergence theory [14, 15]. Detailed steps are as follows:

(1) Initialization: Choose the step number m, and set the parameter $q\,(2 \le q \le m)$ and the precision ε; Choose the initial value $x^{(0)} = 0$, and compute $r^{(0)} = f - A\,x^{(0)}$ $\beta = \| r^{(0)} \|$, $v_1 = r^{(0)} / \beta$, $V_1 = \{ v_1 \}$.

(2) Iteration: For $j = 1, 2, \cdots, m$

1) Incomplete orthogonalization: $h_{ij} = (Av_j\,, v_i)\,(i = j_0, \cdots, j)$, $\hat{v}_{j+1} = Av_j - \sum_{i=j_0}^{j} h_{ij}\, v_i$;

2) Standardization: $h_{j+1,\,j} = \| \hat{v}_{j+1} \|$, $v_{j+1} = \hat{v}_{j+1} / h_{j+1,\,j}$;

3) Renew the matrices V_{j+1} and $\overline{H}_j$

$$V_{j+1} = (V_j, v_{j+1}), \overline{H}_j = \begin{pmatrix} \overline{H}_{j-1} & h_{ij} \\ 0 & h_{j+1,\,j} \end{pmatrix}_{(j+1)\times j}$$

$\overline{H}_j$ is a strip upper Hessenberg matrix. When $j = 1$, the first column is omitted and then $AV_m = V_{m+1}\overline{H}_m$;

(3) Solve the least squares problems $\| r^{(m)} \| = \min_{y_m \in C^m} \| \beta e_1 - \overline{H}_m\, y_m \|$, and obtain y_m;

(4) Construct the approximate solutions $x^{(m)} = x^{(0)} + V_m y_m$;

(5) Compute the modular of residual vectors $\left\| r^{(m)} \right\| = \left\| f - Ax^{(m)} \right\|$;

(6) Restart judgment: If $\left\| r^{(m)} \right\| \le \varepsilon$ and $\varphi(x^{(m)}) < \varphi(x^{(0)})$, $x = x^{(m)}$ is the solution and the iteration is stopped. Otherwise, set $x^{(0)} = x^{(m)}$ and turn to Step(1).

In addition, we presented a novel convergence analysis method that combines theoretical proof with numerical experiments [17]. Through the analysis of the influence of truncation index on the computational efficiency and precision, the IGMRES(m) algorithm has been proved to be rapidly convergent with stable process and high precision. Compared with the GMRES(m) algorithm in other related papers, the IGMRES(m) algorithm has much more excellent convergence condition and computational performances. The IGMRES(m) algorithm and the convergence analysis method are especially suitable for the simulations of elastic and elasto-plastic frictional contact systems and other nonlinear computing systems with complicated and time-consuming iterations.

4 SOME APPLICATIONS OF THE FM-BEM IN ROLLING ENGINEERING

4.1 Large-scale simulations of roll shape and stand stress

4.1.1 Roll shape of the back-up roll

For the back-up roll of a large-scale four-high mill on rigid mount and on rocker bar bearing, their deformations are numerically simulated by the mathematical programming FM-BEM. The roll discrete meshes are shown in Fig.5(a). The number of discrete elements is 5668, and the DOF is 34008. Young's modulus and Poisson's ratio are E＝200 Gpa and μ＝0.3, respectively. The width of contact zone is 14mm. The assumed pressure on the roller surface is 1330Mpa. 36-point Gauss integral is used in the numerical integration.

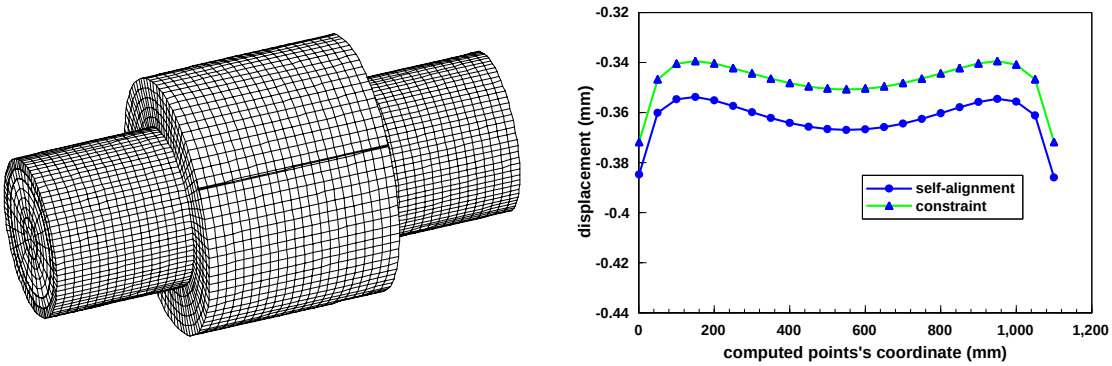

(a) Discrete meshes for the roller (b) Displacements on the roller surface

Fig. 5 Discrete meshes and displacements on the roller surface

After 12 hours, 18 minutes and 16 seconds, the deformations of the roller on two kinds of support are obtained. The deformation curves are shown in Fig.5(b). The results show that the deformation of roller on rocker bar bearing is larger than that of on rigid mount. The increment is less than 1.5%, so it is necessary to consider its influence.

4.1.2 Field of stand stress

By using the mathematical programming FM-BEM, the field of stand stress is numerically simulated. The stand structure and discrete meshes are shown in Fig.6, and the main computing parameters are shown in Table 1. The deformation and stress of the stand are shown in Fig. 7. The maximal tension stresses for the medial surface of the stand upright, the bottom surface of the lower separator and the top surface of the entablature are 8.4MPa, 26MPa and 5.85MPa, respectively. The maximal tension stress 58MPa occurs at the transitional round corner of the bottom surface and the cylinder of the entablature boring. The deformations

on the bottom surfaces of the stand window and the entablature boring are not uniform on the plane. So the average value 0.466mm is taken, which indicates the longitudinal deformation of the stand window.

Table 1 Main parameters

Sectional area of the upright (/cm^2)	Material	Young's modulus (/GPa)	Intensity limitation (/MPa)	Poisson's ratio	Rolling pressure (/MN)	Equilibrant (/KN)
6105	ZG35	210	600	0.3	22	700

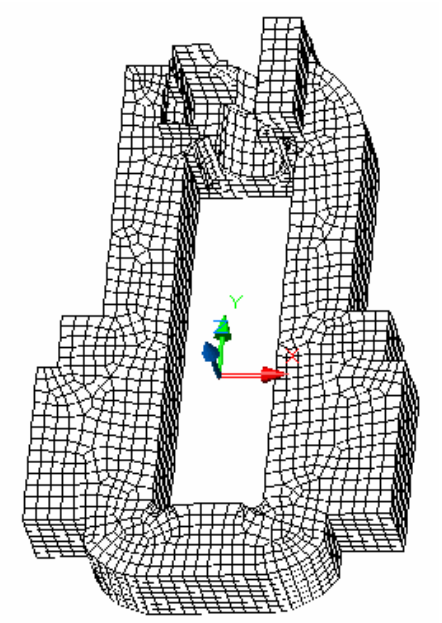

Fig.6 Stand and discrete meshes

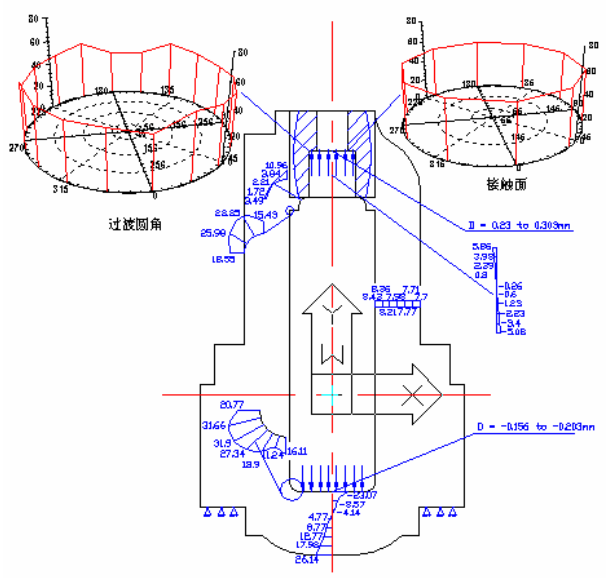

Fig.7 Field of stand stress

4.2 Simulation of the assembly process for large-scale oil film bearing tapered sleeve and roll neck

By using the optimization FM-BEM, the assembly process is demonstrated for the tapered sleeve and roll neck of a large-scale oil film bearing. A roll neck inside a tapered bearing sleeve with an oil-film is the assembly shown in Fig.8 (a). The exterior surface of the tapered sleeve is a cylindrical surface. The taper of the inner surface is $\triangleleft 1:30$, which is the same as that of the neck surface. There is a hydraulic bulge assembly groove seal at each end of the inner surface of the sleeve. In the actual assembly, a "fish tail" and "bonding" phenomena exists. The simulation of contact pressure change is significant not only in theory, but also in engineering practice. During the assembly, the roll neck is fixed, and the tapered sleeve moves 54mm in the axial direction. This results in a magnitude value of 1.8 mm in the radial direction.

Stress concentration occurs near the seal grooves, where meshes of the tapered sleeve and roll neck are subdivided. Their discrete meshes are shown in Fig.8 (b) and (c), respectively. The computing parameters are shown in Table.2. Young's modulus and Poisson's ratio are E＝206 Gpa and μ＝0.3, respectively.

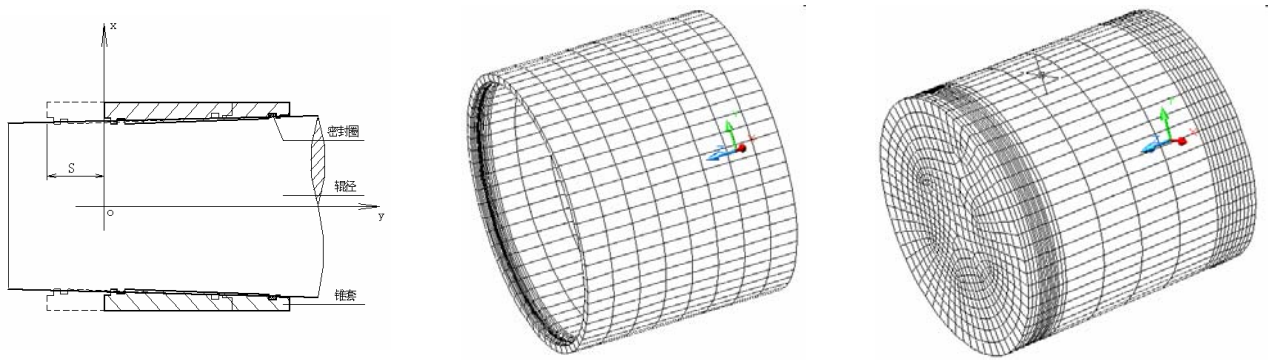

(a) Calculation model (b) Meshes for the tapered sleeve (c) Meshes for the roll neck

Fig.8 Calculation model and discrete meshes

Table 2 Computing parameters

Bodies	Totality		Contact zone		DOF
	Node number	Element number	Node number	Element number	
Tapered sleeve	3120	3120	1380	1200	13500
Roll neck	2854	2852	1500	1440	13062
Total number	5974	5972	2880	2640	26562

When the assembly is fit together, the distribution of the contact pressure is shown in Fig.9(a). In the contact zone, the peak value of contact pressure reaches 678Mpa (It is less than the yield limit of the sleeve, but it is greater than the yield limit of the roll neck 590Mpa.), which is the main reason causing "fish tail" in the roll neck. Therefore, under the current assembly conditions, "fish tail" and "bonding" are inevitable for the sleeve and roll neck.

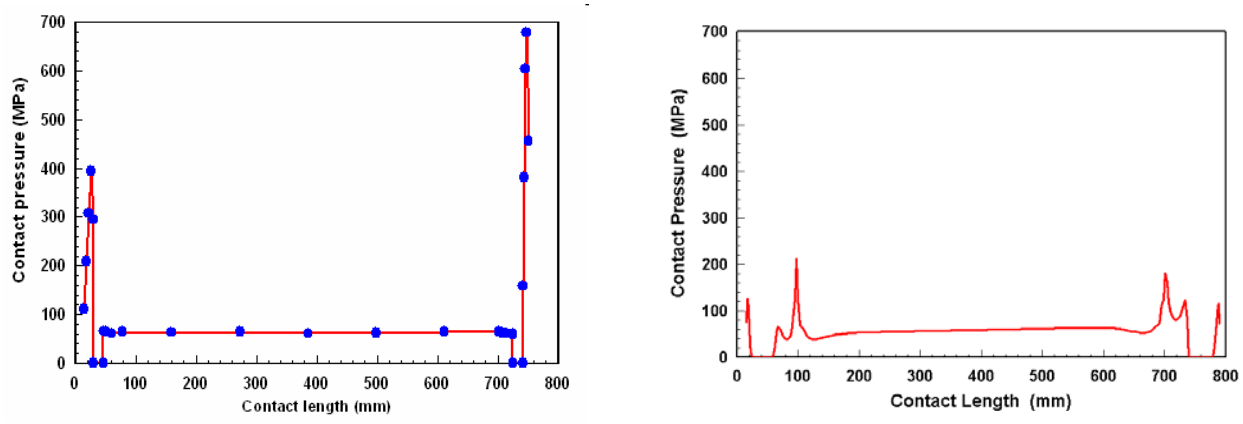

(a) Before optimization (b) After optimization

Fig. 9 Contact pressure

The total load is divided into five incremental steps, and the total computation time is 18 hours and 23 minutes. However, if the FM-BEM without the mathematical programming is used, the convergence is exceptionally slow and no satisfactory results can be obtained (Two incremental steps take more than 30 days).

To improve the stress concentration phenomena in the assembly, we optimize the magnitude of interference for the tapered sleeve, as is shown in Fig.10, where $\Delta\delta_1 = 0.065mm$, $\Delta\delta_1' = 0.03mm$, $\Delta\delta_2 = 0.05mm$, $\Delta\delta_2' = 0.025mm$, $S_1 = S_2 = 36mm$.

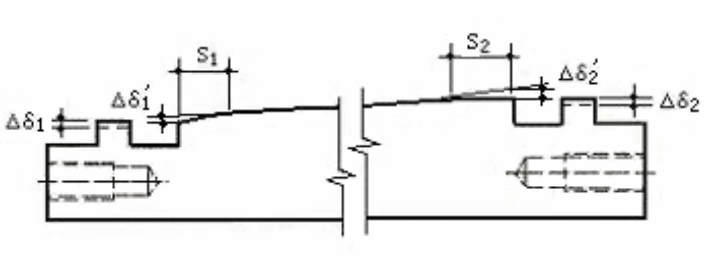

Fig.10 Optimized tapered sleeve

After optimization, the distribution of contact pressure inside of the tapered sleeve is shown in Fig.9(b). The pressures at both ends obviously reduce and the peak value reduces to 210Mpa. It is in the elastic range.

4.3 Reliability analysis of the 3500mm mill pressure screw-pairs

Fig.11 shows the properties of 3500 heavy and medium plate mill press down system. (a) is the structural diagram. (b) and (c) show the thread profile and the pressure screw-pairs profile, respectively.

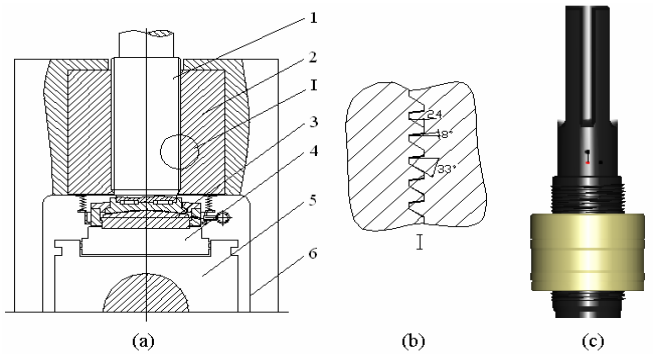

1. Pressure screw 2.Nut 3.Spherical mat 4.AGC 5.Bearing block 6.Stand

Fig.11 3500mm mill pressure screw-pairs

The medium diameter of pressure screw is $d = 656$ mm and the screw pitch is $t = 40$ mm. There are 22 teeth in nut altogether. Material properties and loads are shown in Table.3. The coefficient of friction between teeth is 0.1, which is the static friction value with lubrication.

Table 3 Materials and loads

No.	Properties	Pressure screw	Pressure nut
1	Materials	42CrMo	ZcuCn23Al6Fe3Mn2
2	Young's Modulus E / GPa	206	103
3	Poisson ration ν	0.3	0.3
4	Rolling force Fr / MN	70	70
5	Additional force Fe / MN	1	1

The running clearance and tip clearance of the pressure screw-pairs are 0.167 mm and 0.8 mm, respectively. The computing model is shown in Fig.12(a). The discrete mesh charts for the pressure screw and nut are shown in Fig.12(b). There are altogether 5,390 four nodes linear surface elements (2,696 for screw and 2,694 for nut).

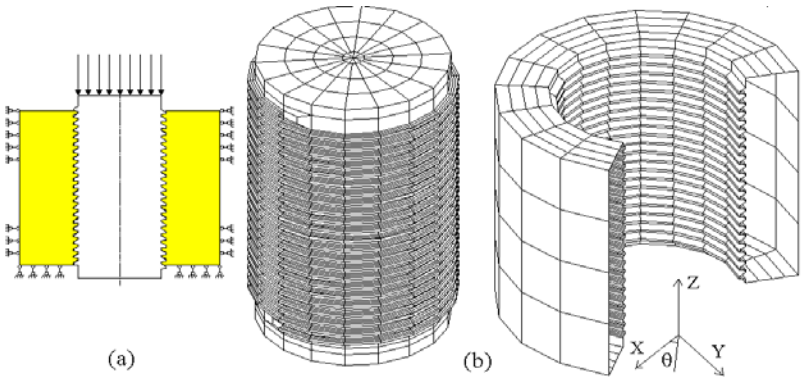

Fig.12 Computing model (a) and discrete meshes (b)

The 3-D traction field in the pressure screw-pair of a 3500 heavy and medium plate mill press down system is successfully calculated by applying the mathematical programming FM-BEM and the corresponding program that has been developed by our group. The main results are shown in Fig.13.

In Fig.13, θ indicates the included angle between the horizontal axial and each cross-section. Line 1 indicates the distribution of circumferential traction under medium-diameter orientation, and line 2 indicates that under interference loads.

The computing results show the medium diameter orientation is unreliable, especially under the interference of an outer force couple. Under such working conditions, the circumferential traction distribution on the screw teeth is extremely uneven, which is the main reason for the destruction and short life time of screw-pairs. Also, the simulation results provide a new tool for designing new pressure screw-pairs whose pressure distribution will be even. When utilizing the same precision (the relative tolerance is 10E-5), the FM-BEM uses almost the same CPU time as used by the FEM, but the needed computer memory size is only

one eightieth of that needed by the FEM (10MB vs. 800MB). The FM-BEM is well suited for computing large-scale engineering problems.

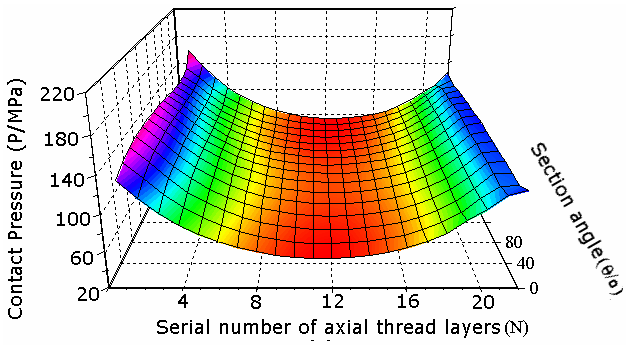

(a) Medium-diameter Orientation

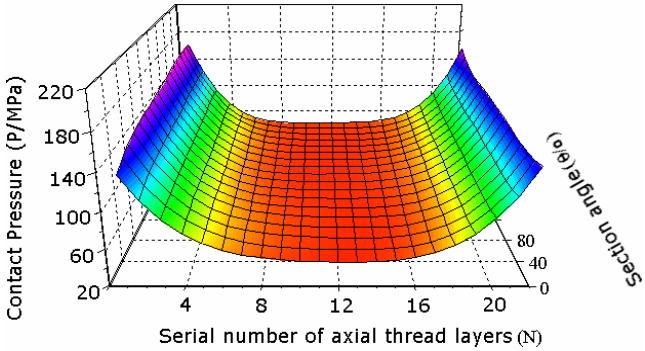

(b) Addendum Orientation

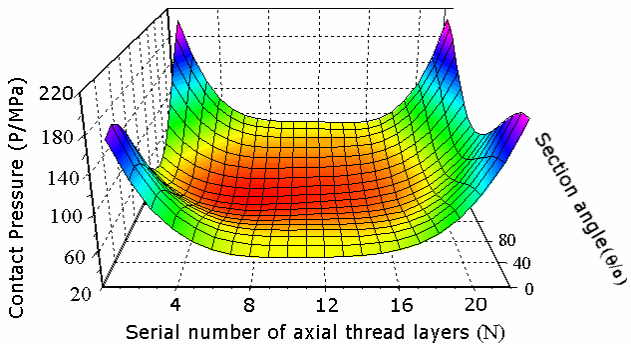

(c) Under partial load

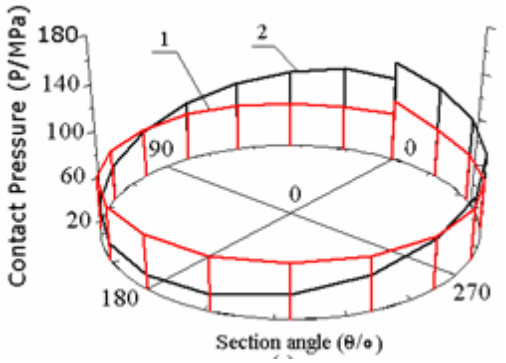

(d) The second circle under partial load

Fig.13 3-D contact stress distributions of the screw teeth

4.4 Numerical simulation of the cold-rolling process of 2030mm four-high mill

Combined with high performance computation and numerical optimization technique, a kind of IGMRES(m) based multi-body network parallel FM-BEM method is proposed. Under PVM network parallel computing platform, related Fortran source programs are developed for large scale computation. The cold-rolling process of 2030mm strip four-high mill is successfully simulated and many satisfactory results are finally obtained. Compared with other related methods and numerical simulations, the computational efficiency and the problem scale are greatly improved.

4.4.1 Multi-body Network Parallel FM-BEM

At first, the network parallel computing environment is established. Then the computing procedure is analyzed and designed for multi-body network parallel FM-BEM. The hardware structure and the software environment for the parallel computing are shown in Fig.14.

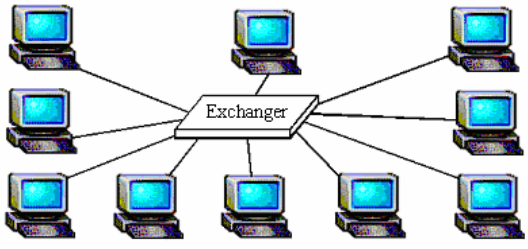

(a)Hardware structure

Development tool: Fortran	Monitoring task supervisor	Parallel platform: PVM
Operating system: Windows 2000		

(b)Software environment

Fig.14 Hardware structure and software environment

4.4.2 Simulation of Cold-rolling Process of Four-high Mill by Using the Network Parallel FM-BEM Method

By using the IGMRES(m) based multi-body network parallel FM-BEM method, 2030mm strip cold-rolling process of four-high mill is simulated. The calculation model and the discrete meshes are shown in Fig.15. The size and rolling parameters for the back-up roll, the working roll and the strip are shown in Table 4.

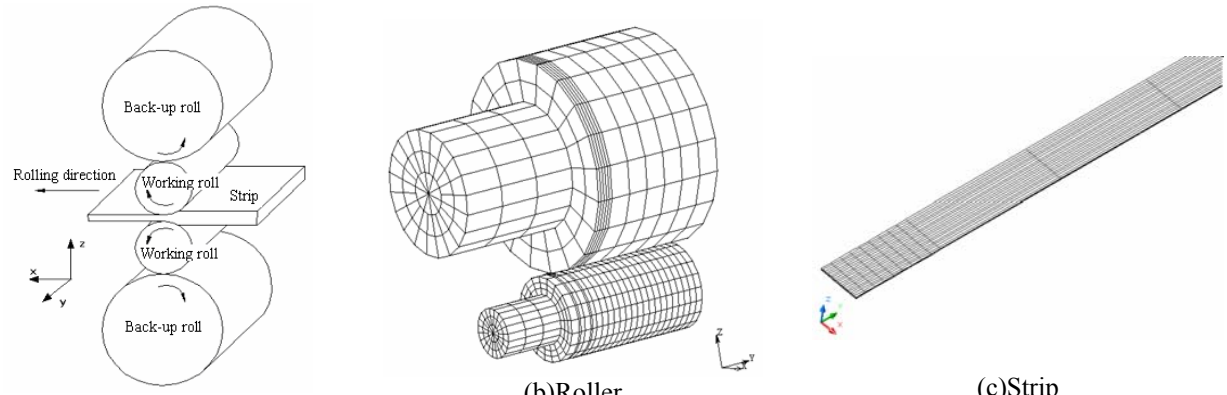

(a)Roll system (b)Roller (c)Strip

Fig. 15 Calculation model and discrete meshes

Table 4 Rolling parameters

Back-up roll		Working roll		Strip	
Young's modulus (E/GPa)	210	Young's modulus (E/GPa)	210	Young's modulus (E/GPa)	206
Poisson ratio (υ)	0.3	Poisson ratio (υ)	0.3	Poisson ratio (υ)	0.3
Roll radius (R/mm)	750	Roll radius (R/mm)	300	Initial thickness (h0/mm)	1.25
Roll body length (L/mm)	2030	Roll body length (L/mm)	2230	Width (b/mm)	1850
Friction coefficient (μ)	0.1	Friction coefficient (μ)	0.1	Friction coefficient (μ)	0.08
Contact tolerance (Δ /mm)	0.001	Contact tolerance (Δ /mm)	0.002	Contact tolerance (Δ /mm)	0.003
--	--	--	--	Yield stress (σ_s /MPa)	250
--	--	--	--	Stiffness coefficient (H)	0.002
--	--	--	--	Press down ratio (%)	20
--	--	--	--	Forward pull (T1/N)	2430

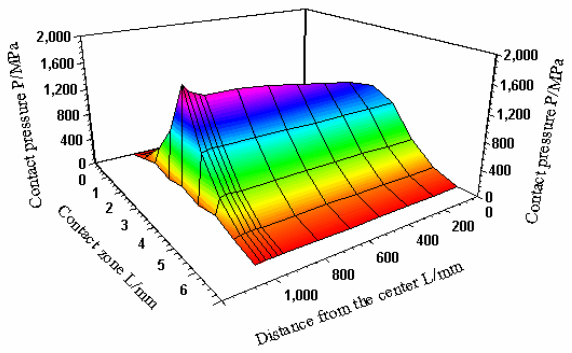

(a)Contact pressure

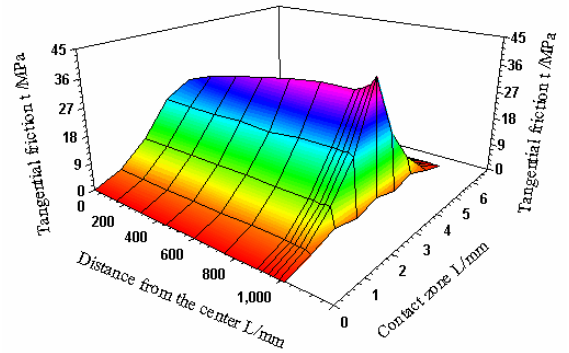

(b)Tangential friction

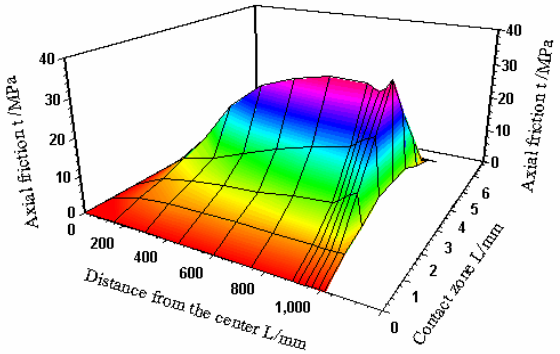

(c)Axial friction

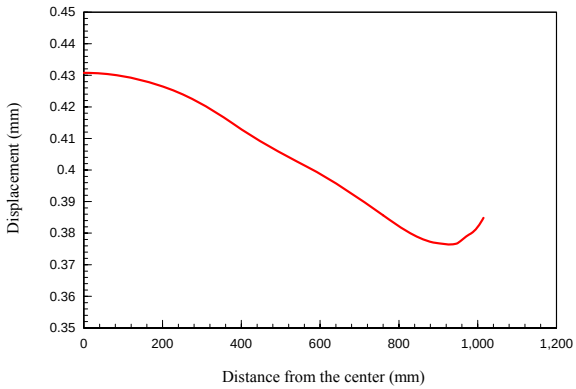

(d)Displacement of the back-up roll

Fig.16 Main computing results

4.4.3 Main Results and Discussions

In the numerical simulation, the presented method is implemented on 10 computers. The truncation ratio is 0.1. After 40 hours and 37 minutes, some final results are obtained for the coupling deformation of the working roll and the back-up roll, as are shown in Fig.16.

In addition, other related numerical simulations have been made by our group. It shows that it is impossible to solve the above rolling problem by traditional BEM. By using the FM-BEM, the final success also can not be achieved because this large computational scale often results in all kinds of troubles and makes the solution be interrupted. Among our simulations, there are two other successful experiments. One is for the strip rolling problem with breadth-thickness ratio 200 by using the network parallel BEM method on 7 computers. The computation lasts more than 5 days. The other one is for the strip four-high mill rolling problem with breadth-thickness ratio 1850 by using the GMRES(m) based network parallel FM-BEM method on 10 computers. The computation time is 42 hours and 24 minutes. These experiments and computational results demonstrate that the IGMRES(m) based network parallel FM-BEM method has greatly improved the computational efficiency and can solve the large scale strip rolling problems with irregular multi-body structures and complex computing conditions.

5 CONCLUSIONS

According to the international progress of the numerical analysis methods, we introduced the FMM into the BEM and preliminarily developed the numerical method of FM-BEM. Also we established some mathematical theories of FM-BEM, presented some practical efficient formulae and algorithms, and mainly applied it into the simulation of rolling engineering. For the study of FM-BEM, different researchers have different viewpoints and they are interested in different application fields. For the present, the studies of FM-BEM have all kinds of specialties. So we can objectively say that the development of FM-BEM is still immature in theory, in numerical method and in applications. Many problems on FM-BEM need us to think about.

In our further investigations, we will address ourselves to the improvement of FM-BEM theory and try to develop it into a kind of mature numerical method. Therefore, it is necessary to abstract the essence from the present FM-BEM in different application fields. This research is significant for the numerical method itself and its service ability of guiding applications.

ACKNOWLEDGEMENTS

The support of the National Natural Science Foundation of China (No.: 50075075) is gratefully acknowledged.

REFERENCES

1. Y.H. Liu, X.F. Zhang and Z.Z. Cen. Lower Bound Limit Analysis of 3-D Elastoplastic Structures by Boundary Element Method. *Applied Mathematics and Mechanics*, 2003; 24(12): 1301-1308.
2. A. Fekih, H. Xu and F. N. Chowdhury. Neural networks based system identification techniques for model based fault detection of nonlinear systems. *IJICIC*, 2007; 3(5): 1073-1085.
3. L. Greengard and V. Rokhlin. A fast algorithm for particle simulations. *J. Comput. Phys.*, 1987; 73(12): 325-348.
4. H.T. Wang, Z.H. Yao and P.B. Wang. On the preconditioners for fast multipole BEM for 2D multi-domain elastostatics. *Engrg Anal Boundary Elements*, 2005; 29(7): 673-688.
5. D.Y. Liu and G.X. Shen. Multipole BEM for 3-D elasto-plastic contact with friction. *Tsinghua Science & Technology*, 2005; 25(1): 57-60.
6. C.X. Yu and G.X. Shen, and D.Y. Liu. Program-pattern multipole boundary element method for frictional contact. *Acta Mechanica Solida Sinica*, 2005; 18(2): 76-82.

7. X.M. Chen, G.X. Shen and D.Y. Liu. Frictional contact multipole-BEM and 3-D analysis of screw pairs. *Chinese Journal of Mechanical Engineering (English Edition)*, 2004; 17(3): 411-414.
8. J.T. Chen and K.H. Chen. Applications of the dual integral formulation in conjunction with fast multipole method in large-scale problems for 2D exterior acoustics. *Engrg Anal Boundary Elements*, 2004; 28(6): 685-709.
9. Y. J. Liu. A new fast multipole boundary element method for solving large-scale two-dimensional elastostatic problems. *Int. J. Numerical Methods in Engineering*, 2006; 65(6): 863-881.
10. Y.J. Liu and Nishimura. The fast multipole boundary element method for potential problems: A tutorial. *Engrg Anal Boundary Elements*, 2006; 30(5): 371-381.
11. Shen G.X., Liu D.Y., and Yu C.X.. *Fast multipole boundary element method and engineering of rolling mill*. Science Publishers, Beijing, 2005.
12. D.Y. Liu and G.X. Shen. 3-D elastic fast Multipole-BEM. *Chinese Journal of Computational Mechanics*, 2004; 21(4): 464-469.
13. C.X. Yu and G.X. Shen. Study on the surface fast multipole boundary element method based on spherical harmonic space. *IJICIC*, 2006; 2(3): 581-591.
14. C.X. Yu. Nonlinear mathematical programming FM-BEM for the elastic frictional contact system. *IJICIC*, 2008; 4(2): 403-412.
15. C.X. Yu and G.X. Shen. Program-iteration pattern Fast Multipole BEM for elasto-plastic contact with friction. *Chinese Journal of Computational Mechanics*, 2008; 25(1): 65-71.
16. C.X. Yu. Existence and Uniqueness of the Solution for FM-BEM Based on GMRES(m) Algorithm. *ICIC-EL*, 2008; 2(1): 89-94.
17. C.X. Yu. Fast Convergent IGMRES(m) Algorithm Based on FM-BEM for Elastic and Elasto-plastic Nonlinear Systems. *IJICIC*, 2009; 5(6): 1785-1794.
18. C.X. Yu, D.Y. Liu and G.X. Shen. Multi-body Network Parallel Nonlinear FM-BEM and the Numerical Simulation. *ICIC-EL*, 2010; 4(1) (in press)